Dan-Yang Ma, Lin-Hai Han, Xiaodong Ji, Wei-Biao Yang. Behaviour of hexagonal concrete-encased CFST columns subjected to cyclic bending. Journal of Constructional Steel Research, 2018, 144: 283-294.

Behaviour of hexagonal concrete-encased CFST columns subjected to cyclic bending

Dan-Yang Ma[a], Lin-Hai Han[a,*], Xiaodong Ji[a] and Wei-Biao Yang[b]

[a]Department of Civil Engineering, Tsinghua University, Beijing, 100084, P.R. China

[b]Beijing Institute of Architectural Design, Beijing 100045, P.R. China.

ABSTRACT

The hexagonal concrete-encased CFST column consists of a CFST (concrete-filled steel tube) core and a hexagonal-shaped reinforced concrete (RC) encasement. This paper presents the finite element (FE) analysis of hexagonal concrete-encased CFST columns subjected to axial compressive forces and cyclic bending moments. High-fidelity finite element analysis (FEA) model is established and validated by comparison with the test data in terms of failure mode and hysteretic curves. From the FEA model, the hysteretic response of the composite columns, the contact stress between the steel tube and concrete, and the strength contribution of different components during the full range of loading are illustrated. Parametric analysis is conducted to investigate the influences of various parameters on force-displacement envelope curves of the hexagonal concrete-encased CFST columns. The parameters include the material strength, confinement factor of CFST section, stirrup characteristic value, area ratio of CFST core to RC encasement, and axial force ratio. Finally, simplified methods are proposed to predict the flexural strength of hexagonal concrete-encased CFST columns. The predictions from simplified methods showed good agreement with the experimental and analytical results.

KEYWORDS: Concrete-encased CFST; Hexagonal section; Cyclic behaviour;

Please cite this article as: Dan-Yang Ma, Lin-Hai Han, Xiaodong Ji, Wei-Biao Yang. Behaviour of hexagonal concrete-encased CFST columns subjected to cyclic bending. Journal of Constructional Steel Research, 2018, 144: 283-294.
Doi: 10.1016/j.jcsr.2018.01.019

Full-range analysis; Strength prediction

*Corresponding author: Professor Lin-Hai Han, Department of Civil Engineering, Tsinghua University, Beijing, 100084, China. Tel & Fax: 86 10 62797067. E-mail addresses: lhhan@tsinghua.edu.cn (L-H Han)

NOTATION

A	Cross-sectional area of concrete-encased CFST
A_{core}	Cross-sectional area of CFST core
$A_{\mathrm{e,out}}$	Equivalent area of outer concrete
B	Side length
D	Distance to the middle axis
E_{s}	Modulus of elasticity of steel
E_{c}	Modulus of elasticity of concrete
f_{c}'	cylinder strength of core concrete
$f_{\mathrm{c,core}}$	Prismatic strength of core concrete
$f_{\mathrm{c,out}}$	Prismatic strength of outer concrete
$f_{\mathrm{cu,core}}$	Cube strength of core concrete
$f_{\mathrm{cu,out}}$	Cube strength of outer concrete
f_{ys}	Yield strength of steel tube
f_{yl}	Yield strength of longitudinal rebar
f_{yh}	Yield strength of stirrup
M_{RC}	Flexural strength of the RC encasement component
M_{CFST}	Flexural strength of CFST component
M_{u}	Flexural strength
M_{uc}	Predicted flexural strength
M_{ue}	Measured flexural strength
n	Axial force ratio
N_0	Constant axial load
N_{u}	Compressive strength
P	Lateral load
P_{uc}	Predicted ultimate strength
P_{ue}	Measured ultimate strength
s	Stirrup spacing
t	Steel tube thickness of CFST
α	Area ratio of CFST core
α_{s}	Steel ratio of CFST core
β	Factor of equivalent rectangular stress block
Δ	Displacement
Δ_{y}	Yield displacement
Δ_{u}	Ultimate displacement
θ	Drift ratio
θ_{u}	Ultimate drift ratio
λ_{v}	Stirrup characteristic value
ρ_{v}	Volumetric stirrup ratio
ρ_{s}	Longitudinal rebar ratio
ξ	Confinement factor for CFST section

1. Introduction

CFST consists of the steel tube filled with concrete. CFST members with hexagonal cross section are used in some high-rise buildings for their aesthetic performance, where the members act as mega columns in the mega frame-core wall systems [1]. Moreover, the hexagonal shape makes the column easier to be connected with beams and the core wall. In the past, the performance of hexagonal CFST column members under axial compression and bending has been investigated by Xu et al.[1]. The CFST component is found to have increased compressive strength and ductility.

The concrete-encased CFST column consists of an inner CFST component and an outer reinforced concrete encasement component. The steel tube can provide confinement to the core concrete, and the reinforced concrete encasement can provide fire protection and corrosion protection. Because of these benefits, the concrete-encased CFST column has been increasingly used in high-rise buildings and bridges in China [2], such as Baoli Square of Shanghai, Jialing River Bridge and Labajin Bridge. The cross sections of the concrete-encased CFST column are usually circle, square, and rectangular for an easy beam-to-column connection. Han et al. [3] conducted experimental tests on concrete-encased CFST columns with aforementioned cross section. Ji et al. [4, 5] reported a series of experiments on the seismic performance of concrete-encased CFST columns with square section. Both sets of tests indicate that concrete-encased CFST columns have favorable ductility and energy dissipation. Qian et al. [6] presented an analytical study on the cyclic behaviour of concrete-encased CFST columns with square section. In some complicated structures like China Zun, the highest building in Beijing, the column is not only connected to beams and shear wall in the longitudinal direction or transverse direction, but also in the diagonal direction. In such a circumstance, the hexagonal column section is convenient to be connected to beams and shear wall. The concrete-encased CFST column with a hexagonal section is designed to be applied in that circumstance. However, the research on the hexagonal concrete-encased CFST columns is very limited. The whole response of the hysteretic curve, the contact stress between steel tube and concrete, and the strength contribution of different components of the hexagonal concrete-encased CFST column have yet to be clearly understood.

To this end, the main objectives of this research are thus threefold: (1) To develop a high-fidelity finite element analysis (FEA) model that can accurately represent the cyclic behaviour of the hexagonal concrete-encased CFST column; (2) To conduct full-range analysis of the hexagonal concrete-encased CFST column, for estimating the contact stress between steel tube and concrete, and the strength contribution of different components; and (3) To establish a simplified model for the flexural strength prediction of the hexagonal concrete-encased CFST column.

2. FEA model

A FEA model was developed using ABAQUS/Standard module [7] to represent the specimen of hexagonal concrete encased CFST column in Xu [8]. Using the symmetricity, a quarter model was considered.

The schematic view of the FEA model of the hexagonal concrete-encased CFST is shown in Fig. 1. This type of cross section is chosen to be a “standard” hexagonal shape in this study. The dual-axisymmetric cross section has an equal side length (B) for each edge of CFST core, two interior angles of 90° (θ_1) and four interior angles of 135° (θ_2).

2.1 Material properties

The concrete damaged plasticity model was used to simulate the behaviour of the concrete under cyclic loading. The concrete section was divided into three regions according to different levels of confinement, as shown in Fig. 1(a). The uniaxial compressive strain-stress relation of the core concrete, outer stirrup-confined concrete and concrete cover were simulated by the constitute models proposed by Han et al. [9], Han and An [10] and Attard and Setunge [11], respectively. Note that there is no specific constitute model for the core concrete of the hexagonal CFST. The axial compressive behaviour of the hexagonal CFST[1] and rectangular CFST[12] was compared by experimental tests. Both sets of CFST columns for comparison had similar confinement factor ξ (= $\dfrac{\alpha_{\mathrm{s}} f_{\mathrm{ys}}}{f_{\mathrm{ck,core}}}$) and compressive strength of core concrete $f_{\mathrm{c}}'_{\mathrm{,core}}$. The experimental results are shown in Fig. 2. The hexagonal CFST specimens were named by “C”, and the rectangular CFST specimens by “rc”. It can be concluded that the axial strain-force relationship curves of two different sections are similar, which means the uniaxial compressive model of core concrete for the rectangular CFST can be used for the hexagonal CFST. The uniaxial compressive model of core concrete for the rectangular CFST is used for the core concrete with the hexagonal section. The uniaxial tensile model suggested by Shen et al.[13] is used for three types of concrete. The elastic modulus E_c and Possion's ratio of concrete are taken as $4730\sqrt{f_c^{'}}$ and 0.2 respectively according to ACI318-11 [14], where f_c' is cylinder compressive strength in MPa.

The longitudinal rebars are simulated using Clough model[15]. The steel tube and stirrups are simulated using combined hardening model as shown in Fig. 3. The Clough model is used for the reason that the slippage between longitudinal rebars and concrete does not directly simulate in the FEA model. The Clough model can take into account the slippage effect to some degree. The combined hardening model can simulate Bauschinger effects of steel tube. The parameters of the combined hardening model are determined by Han et al. [16].

2.2 Interaction, Boundary condition, and Element mesh

As the concrete damaged plasticity model cannot capture the opening and closure of concrete cracks[17], a discrete crack between the concrete and the restricted part is introduced to simulate this effect. The discrete crack is represented by the contact pair in ABAQUS, where the "hard" contact is used in the normal direction and the Coulomb friction is used in the tangential direction. The frictional factor μ of the Coulomb friction is taken as 1.0 according to the provisions of ACI 318-14[14].

The interaction between the steel tube and concrete is simulated by the surface-to-surface contact interaction, where the "hard" contact is applied in the normal direction and the Coulomb friction with a frictional factor of 0.6 is applied in the tangential direction. The parameters of the contact interaction model have been verified by past researchers[6]. The end plate and steel tube are rigidly connected by "tie" constraint in ABAQUS, and the end plate is connected to the concrete by "tie" constraint as well. The rebars are connected to the outer concrete using the "embedded" constraint. The interactions between different components can be seen in Fig. 1.

2.3 Verifications of the FEA model

The FEA model is verified by the cyclic test results of square concrete-encased CFST columns by Ji et al. [4] and hexagonal concrete-encased CFST columns presented in Xu[8].

The specimen CCS3 and CCS4 from the experiments conducted by Ji et al. [4] had a square section of 300 mm by 300 mm. A circular steel tube was embedded in the concrete and the confinement factor was 1.01. A vertical load was applied to the specimen at the beginning of the test and maintained constant. Cyclic loads were applied quasi-statically by the horizontal actuator. The major difference between the two specimens is the amount of stirrups. The specimen CCS3 has a closer stirrup spacing than specimen CCS4. Two specimens showed a flexural failure mode, characterized by the yield of the longitudinal rebars and compressive crushing of the concrete at the plastic hinge of the column specimens.

In the design of Xu's experiment, the flexural strength and shear strength were predicted. The flexural strength was calculated by the strength prediction method proposed by An and Han[18], which is based on the assumption that a plane remains plane after bending. The shear strength was calculated by the formula according to CECS188[19]. The shear force corresponding to the calculated flexural strength of the specimen is 122.9 kN, much lower than the calculated shear strength capacity of 482.6 kN. The experimental section and test setup for Xu's test[8] is shown in Fig. 4. The column was pin connected to the loading setup. The foundation was securely fixed to the strong floor. The axial force was loaded by a horizontal jack. The axial compressive load was firstly applied and maintained constant. The axial force ratio n ($=N_0/N_u$) was equal to 0.1, where N_u denotes the compressive strength calculated by the formula proposed by Han and An[10]. Afterwards, the cyclic vertical load was applied at the column mid-span along the strong axis of the column's cross section. Before the specimen yielded, the vertical loading was force controlled, and then it was changed to the displacement controlled till the failure of the specimen. Three force magnitudes were considered in the force-controlled loading, i.e., 28, 56 and 84 kN. The amplitude increment of displacement controlled loading was 2mm. Note that the vertical displacement of pin connection at the column ends, induced by the local rotation of the loading jack, would lead to an additional vertical displacement at the column mid-span. To reflect this effect, a shear linear spring was added beyond the end plate along the vertical direction in the FEA model, and the spring stiffness parameter was determined by matching the initial stiffness value of the FEA model with the test results.

Table 1 summarizes the FEA results, compared with the test results. The mean value and the standard deviation of P_{ue}/P_{uc} are 1.0 and 0.009, respectively, which indicates that the FEA model could predict the ultimate strength reasonably. The predicted yield displacement Δ_y and ultimate displacement Δ_u also correlated well with the test values. Note that the yield displacement Δ_y is determined according to Priestley and Park[20]. Fig. 5 shows the photographs of specimens after testing and the predicted failure mode from the FEA model. Fig. 6 compared the calculated and experimental hysteretic curves of the specimens. The predicted values of the loading and unloading stiffness are close to the measured values, and the pinching phenomenon is reflected as well.

3. Analytical behaviour

A typical numerical sample for hexagonal concrete-encased CFST column is established using the verified FEA model. The dimensions and loading procedure of the model are identical to the test specimen in Xu[8]. The axial force ratio is 0.15. The commonly-used material strengths for the concrete-encased CFST columns are considered in the analysis. The material strengths are: $f_{cu,out}$ = 40 MPa; $f_{cu,core}$ = 60 MPa; f_{ys} =345 MPa; f_{yl} =335 MPa and f_{yh} = 335 MPa. Note that Chinese codes use the cubic compressive strength for grading concrete, which can be transferred to cylinder compressive strength by linear interpolation[21].

3.1 Analysis of load-displacement relation

Fig. 7 shows the typical hysteretic curve and envelope curve of the hexagonal concrete-encased CFST column. Four characteristic points, i.e. A, B, C and D are denoted in the curve to analyze the behaviour of the hexagonal concrete-encased CFST column in different stages as follows: (1) Point A, initial yielding of the longitudinal rebar; (2) Point B, initial yielding of the steel tube and spalling of concrete cover; (3) Point C, the maximum strength; (4) Point D, the strength decreased to 85% of the maximum strength.

(1) Point A

Point A indicates the yielding of the longitudinal rebar. The secant stiffness of the composite column at Point A is 0.48 of the initial stiffness. The stress distributions of longitudinal rebars are shown in Fig.8 (a), and the yielding of rebars are concentrated in the junction of the restricted part and other parts. The maximum width of the discrete crack reaches 0.36 mm at point A. Fig.8 (b) indicates that the neutral axes of outer concrete and core concrete are at the same height at point A. The outer concrete has reached the uniaxial compressive strength in the longitudinal direction, while the longitudinal stress of core concrete is lower than half of the uniaxial compressive strength. The steel tube is in the elastic stage.

(2) Point B

Point B indicates the yielding of the steel tube. The von Mises stress of the steel tube is shown in Fig.9 (a). The tensile edge and the compressive edge of the steel tube yield almost simultaneously. The steel tube develops the largest von Mises stress in the section that is approximately 60 mm apart from the restricted part, in which the concrete develops the largest plastic strain for the section is at the middle of two stirrups. Therefore the section of 60 mm away from the junction is selected as the governing section. The longitudinal stress of steel tube and concrete in the governing section are shown in Fig.9 (b). The steel tube has largest longitudinal stress at point a and point d, and the longitudinal stress varies gradually from point a to point d. The stresses in red represent the post-peak stresses, while those in black represent the stresses prior to the maximum strength. The spalling of the concrete cover is also found at this typical point. The maximum longitudinal strain of the concrete is 4585με, exceeding the spalling strain of concrete cover[22]. The longitudinal stress of core concrete reaches the uniaxial compressive strength.

(3) Point C

Point C indicates the maximum strength of the specimen. The longitudinal stress of concrete and steel tube at governing section is shown in Fig.10 (a). The longitudinal stress of core concrete exceeds the uniaxial compressive strength at this point, indicating that the confining effect induced by the steel tube can further increase the uniaxial compressive strength. The longitudinal stress of outer concrete decreases to lower than 50% of the maximum strength. Fig.10 (b) shows the longitudinal strain distribution of outer concrete, core concrete, steel tube and rebars at the governing section. The horizontal ordinate *D* means the distance from the measured point to the middle axis. It can be found that the neutral axes of all components are nearly 15mm away from the middle axis and the strain varies linearly along the height of cross section. Except for the post-peak stresses region, the longitudinal strain of concrete cover keeps linear. In the point C, the assumption that a plane remains plane after bending exists for most regions of the whole section.

(4) Point D

Point D indicates the bearing capacity decreases to 85% of the ultimate strength. Fig.

11 (a) shows the equivalent plastic strain of outer concrete. It can be found that the equivalent plastic strain of outer concrete is concentrated in the farthest corners. The stirrups have not yielded yet, and they can provide increasing confinement up to further loading. Fig. 11 (b) shows the stresses of concrete in the *y* direction. The neutral axis of core concrete and that of the outer concrete are not identical. The compressive stress of most outer concrete drops below $0.2f_{c,out}^{'}$. It indicates the bending moment is mostly undertaken by the core concrete in compression and reinforcements in tension. Fig.11 (c) shows the contact stress between the steel tube and concrete. The stresses in blue represents the contact stress between the steel tube and outer concrete, and the stresses in green represents the contact stress between the steel tube and core concrete. The contact stress between the steel tube and outer concrete is found on the compressive side, which means the outer concrete can prevent the steel tube from local bulking under compression. The contact stress between the steel tube and core concrete is distributed at the compressive side and the tensile side, which indicates the steel tube can provide confinement to core concrete under compression and tension.

3.2 Contact stress between steel tube and concrete

The contact stress between steel tube and concrete is discussed in this section, and it is illustrated in Fig. 12. Under positive loading, points 1 and 2 marked in Fig. 12 are subjected to tensile strain and compressive strain, respectively.

The contact stresses of point 1 and point 2 have a similar tendency due to the symmetricity, and the point 3 has little contact stress. The contact stress between steel tube and core concrete represents the confinement to core concrete. The contact stress between the steel tube and core concrete increases with the increase of displacement at the tensile and the compressive edge until $3\Delta_y$ is reached, and the maximum strength of the column is also reached at $3\Delta_y$. The contact stress between the steel tube and outer concrete reaches the maximum value at the compressive edge when the maximum strength of the column is reached. At that instant, the maximum longitudinal strain of the outer concrete is 8458με. The severe damage of outer concrete leads to the decrease of the contact stress between the steel tube and outer concrete. The maximum longitudinal strain of the steel tube is 5034με and it has local buckling due to the decreasing of contact stress between the steel tube and outer concrete. The yielded steel tube couldn't provide more confinement to the core concrete and the core concrete fails gradually, which consequently leads to the decrease of contact stress between the steel tube and core concrete.

In conclusion, the outer concrete can prevent the steel tube from local buckling, and the steel tube can provide the confinement to the core concrete under both tensile and compression before the maximum strength is reached.

3.3 Strength contribution of different components

Fig. 13 shows the contributions of CFST component and RC encasement component on the axial force, shear force and bending moment during the full range of loading on the hexagonal concrete-encased CFST column.

It can be seen from Fig. 13 (a) that the variation trend of axial force is opposite between the CFST component and RC encasement component. The RC encasement component bears a major portion of the axial load before the yield displacement. Afterwards, the axial force carried by the outer RC encasement gradually transfers to the CFST component due to the strength degradation of outer concrete. In the end of loading, more than 50% of the axial load is carried by CFST component. As shown in Fig. 13 (b) and (c), the shear force and bending moment carried by CFST component keep increasing until two times of yield displacement. While the shear force and bending moment carried by the RC encasement component decrease after the yield displacement. The shear force and bending moment carried by the CFST component don't decrease until the end of loading, which ensures a good ductility for the concrete-encased CFST column.

4. Parametric analysis

The major design parameters that affect the cyclic behaviour of the hexagonal concrete-encased CFST column include: (1) cube strength of core concrete ($f_{cu,core}$); (2) cube strength of outer concrete ($f_{cu,out}$); (3) confinement factor for CFST section (ξ); (4) stirrup characteristic value (λ_v); (5) area ratio of CFST core (α); (6) axial force ratio (n). To reflect the variation of those parameters, the material strength, the geometric dimension and the axial force ratio of the FEA model vary as follows: $f_{cu,core}$ = 40-80 MPa; $f_{cu,out}$ = 40-60 MPa; f_{ys} = 235-420 MPa; t = 2-6 mm; f_{yh} = 300-400 MPa; s = 45-135 mm; A_{core} = 16080-34142mm^2; n = 0.15-0.45. The effects of different parameters on envelope curves are shown in Fig. 14. When changing the value of a parameter to investigate its effect, the values of other parameters keep constant and are the same as the values defined in the previous section. The load is applied along the strong axis of the column section, while the loading along the weak axis is not discussed here.

(1) Effects of the concrete strength

In practice, the core concrete of the hexagonal concrete-encased CFST columns is usually designed with a cubic compressive strength of 40-80 MPa, and the outer concrete with a cubic compressive strength of 30-50 MPa. Fig. 14 (a) and (b) show the effects of the compressive strength of core concrete and outer concrete on *P-Δ* envelope curves. The increase of the compressive strength of core concrete $f_{cu,core}$ leads to a slight increase of the maximum strength of the composite column, while it does not influence the post-peak strength deterioration. The increase of the compressive strength of outer concrete $f_{cu,out}$ can increase the bearing capacity of the hexagonal concrete-encased CFST column, while it nearly has no influence on its post-peak behaviour.

(2) Effects of the confinement factor for CFST section (ξ)

Fig. 14 (c) shows the effects of the confinement factor for the CFST section ($\xi=\dfrac{\alpha_s f_{ys}}{f_{ck,core}}$) on *P-Δ* envelope curves. The confinement factor is varied by changing the thickness of steel tube and the yield strength of steel tube. The ultimate strength obviously increases with an increase of ξ, which is related to the steel ratio of CFST core and the yield strength of steel tube. The ultimate strength increases by 15% as the confinement factor for CFST section (ξ) increases from 0.610 to 1.195. Due to the increase of the confining effect, when the confinement factor ξ increases from 0.610 to 1.195, the drift ratio θ_u increased by 115%.

(3) Effects of the stirrup characteristic value (λ_v)

The stirrup characteristic value λ_v specified in GB 50011-2010[23] (i.e., the mechanical volumetric ratio ω_{wd} specified in Eurocode 8[24]) is calculated as $\lambda = \rho_v f_{yv}/f_{c,out}$, where f_{yh} and $f_{c,out}$ denote the yield strength of transverse reinforcement and the axial compressive strength of outer concrete, respectively. Fig. 14 (d) shows the effects of the stirrup characteristic value λ_v on the P-Δ envelope curves. The stirrup characteristic value λ_v is varied by changing the yield strength of stirrup f_{yh} and the stirrup spacing s. The yield strength of the stirrup f_{yh} only has moderate effects on the P-Δ envelope curves when it varies from 235 MPa to 335 MPa. The reason is that the stirrup doesn't yield until the ultimate displacement Δ_u is reached. The decrease of the stirrup spacing s can effectively increase the ultimate displacement. The ultimate drift ratio θ_u increases from 0.016 to 0.024 when the stirrup spacing decreases from 135mm to 45mm.

(4) Effects of the area ratio of CFST core (α)

The area ratio of CFST core α represents the ratio of cross-sectional area of the CFST core to that of the composite column. Fig. 14 (e) shows the effects of the area ratio of CFST core α on P-Δ envelope curves. When the area ratio of CFST core α increases by 0.2, the ultimate strength increases by 13% and the ultimate displacement increases by 40.7%. As the CFST can provide high bearing capacity and ductility, the hexagonal concrete-encased CFST column can have larger ultimate strength and ductility with a larger area ratio of CFST core α.

(5) Effects of the axial force ratio (n)

Fig. 14 (f) shows the effects of the axial force ratio *n* on the *P-Δ* envelope curves. With the axial force ratio *n* varies from 0.15 to 0.45, the flexural strength hardly changes. According to *M-N* interaction diagram analysis of typical column sections, the flexural strength capacity of a RC column significantly increases when the axial force ratio increases from 0 to 0.3, and then the flexural strength capacity of RC column drops down sharply with the further increase of axial force ratio. The *M-N* interaction diagram of the hexagonal concrete-encased CFST column does not have a sharp decrease in flexural strength capacity with the axial force ratio increasing from 0 to 0.45. Similarly as the RC component, the increase of the axial force ratio of the hexagonal concrete-encased CFST column leads to an obvious decrease of ultimate drift ratio. The ultimate drift ratio varied from 0.018 to 0.011 when the axial force ratio *n* increases from 0.15 to 0.45.

Xu et al. [25] has proposed a simplified method to predict the flexural strength of concrete-encased column base. The simplified method was verified by the test results and is modified here to predict the flexural strength of the hexagonal concrete-encased CFST column. The CFST component and RC encasement component bear axial force and bending moment together, which has also been verified by the analytical studies. The following assumptions are made. (1) Linear stain distribution is developed for the section, which has been verified by analytical studies. (2) The ultimate compressive strain ε_{cu} of outer concrete is taken as 0.003[14], and the tensile contribution from the concrete is ignored. (3)Uniform concrete stress is assumed over a compressive zone, where the equivalent stress block area of outer concrete $A_{e,out}$ is calculated according to ACI 318-14[14]. (4) The constitutive model proposed by Han et al.[26] is used for the core concrete. (5) The constitutive model of steel tube and longitudinal rebars follows a bilinear model, and the hardening modulus is $0.01E_s$.

The strain distribution of the whole section can be calculated by the strain at the compressive edge and the compressive zone depth c. The strain and stress distribution are shown in Fig.15. By dividing the whole section into equivalent blocks, the axial force of the RC encasement component (N_{RC}) and CFST component (N_{CFST}) can be calculated as follows:

$$N_{\mathrm{RC}} = 0.85 f'_{\mathrm{c,out}} A_{\mathrm{e,out}} + \sum \sigma_{\mathrm{ri}} A_{\mathrm{ri}} \quad (1)$$

$$N_{\mathrm{CFST}} = \sum \sigma_{\mathrm{c,core}} A_{\mathrm{c,core}} + \sum \sigma_{\mathrm{si}} A_{\mathrm{si}} \quad (2)$$

$A_{e,out}$ is the equivalent area of the outer compressive concrete. As the equivalent area of the hexagonal section has not been investigated, the factor of 0.85 and β for the rectangular section proposed by ACI 318-14[14] are used for the calculation of the compressive strength and height of the equivalent compressive stress block ; σ_{ri} is the stress of a longitudinal rebar; A_{ri} is the cross-sectional area of a longitudinal rebar; $\sigma_{c,core}$ is the stress of a core concrete block; $A_{c,core}$ is the area of a core concrete block; σ_{si} is the stress of a steel tube block. A_{si} is the area of a steel tube block. The maximum strength corresponds to the instant when the extreme compressive edge arrives at the ultimate compressive strain ε_{cu} that is taken as 0.003[14]. From the equilibrium of the axial forces, the compressive zone depth c can be determined using Eq. (3).

$$N_{\mathrm{RC}} + N_{\mathrm{CFST}} = N_{\mathrm{u}} \quad (3)$$

The flexural strength of the RC encasement component (M_{RC}) and CFST component

(M_{CFST}) can be calculated as follows:

$$M_{\mathrm{RC}} = 0.85 f'_{\mathrm{c,out}} A_{\mathrm{e,out}} \left(0.5H - x_{\mathrm{c,out}}\right) + \sum \sigma_{\mathrm{ri}} A_{\mathrm{ri}} \left(0.5H - x_{\mathrm{ri}}\right) \tag{4}$$

$$M_{\mathrm{CFST}} = \sum \sigma_{\mathrm{c,core}} A_{\mathrm{c,core}} (0.5H - x_{\mathrm{c,core}}) + \sum \sigma_{\mathrm{si}} A_{\mathrm{si}} \left(0.5H - x_{\mathrm{si}}\right) \tag{5}$$

Where H is the height of the cross section; $x_{\mathrm{c,out}}$ is the distance from the extreme compressive edge to the centroid of outer compressive concrete. $x_{\mathrm{c,core}}$ is the distance from the extreme compressive edge to the centroid of core concrete block; x_{ri} is the distance from the extreme compressive edge to longitudinal rebars; x_{si} is the distance from the extreme compressive edge to the centroid of steel tube block. Then, the ultimate moment M_{u} can be calculated by using the following expression

$$M_{\mathrm{u}} = M_{\mathrm{RC}} + M_{\mathrm{CFST}} \tag{6}$$

In this paper, Fibre model method, which is achieved by Xtract software, is used to make a comparison with the simplified method. The constitute models proposed by Attard and Setunge[11] and Han et al.[26] are used for the outer concrete and core concrete. The bilinear model is used for the fibres that represent the steel tube and rebars.

The calculated flexural strength (M_{uc}) using the simplified method and fibre model are compared with the measured flexural strength (M_{ue}) in Fig. 16. Both the FEA model and experimental results are used to verify the strength prediction method. Mean values ($M_{\mathrm{uc}}/M_{\mathrm{ue}}$) of 0.838 and 0.946 with the standard deviation of 0.038 and 0.029 are obtained individually for the simplified method and fibre model method. Both methods give reasonable predictions. In conclusion, the proposed simplified method is convenient for manual computation and the fibre model is convenient for computerized calculation.

5. Conclusions

The following conclusions are drawn based on the studies:

(1) A FEA model is developed to represent the hexagonal concrete-encased CFST column. The cracking and damage of concrete, the cyclic behaviour of steel tube, the slippage between longitudinal rebars and concrete, and the interaction between steel tube and surrounding concrete are considered in this model. Comparisons between experimental and FEA results indicate that the FEA model can reasonably track the experimental behaviour of the hexagonal concrete-encased CFST column.

(2) Using the verified FEA model, the hysteretic response of the composite columns, the contact stress between steel tube and concrete, and the strength contribution of different components during the full range of loading are investigated. It is found that, with the increase of lateral displacement, the axial load and bending moment carried by the RC encasement component gradually transfer to the CFST component.

(3) The parametric study shows that the confinement factor for CFST section, stirrup spacing, area ratio of CFST core and axial force ratio have obvious influence on the envelope curve. The maximum strength of the column increases with an increase of the steel tube ratio due to the strength and confinement effects provided by the steel tube. The drift ratio θ_u increases by 115% when the confinement factor ξ increases from 0.610 to 1.195. The ultimate drift ratio θ_u increases from 0.016 to 0.024 when the stirrup spacing decreases from 135mm to 45mm. The ultimate strength increases by 13% and the ultimate displacement increases by 40.7% when the area ratio of

CFST core α increases by 0.2. The confinement provided by the steel tube and stirrups can improve the flexural strength and ductility of the composite column.

(4) In general, the proposed simplified method can provide a reasonable and conservative estimation of the hexagonal concrete-encased CFST columns. The fibre model using X-tract software also can accurately predict the flexural strength of the composite columns.

Acknowledgements

The research reported in this paper is part of the Project 51678341 supported by the National Natural Science Foundation of China (NSFC). The financial support is highly appreciated.

References

[1] W. Xu, L.H. Han, W. Li, Performance of hexagonal CFST members under axial compression and bending, Journal of Constructional Steel Research 123 (2016) 162-175.

[2] L.H. Han, W. Li, R. Bjorhovde, Developments and advanced applications of concrete-filled steel tubular (CFST) structures: Members, Journal of Constructional Steel Research 100 (2014) 211-228.

[3] L.H. Han, F.Y. Liao, Z. Tao, Z. Hong, Performance of concrete filled steel tube reinforced concrete columns subjected to cyclic bending, Journal of Constructional Steel Research 65(8-9) (2009) 1607-1616.

[4] X. Ji, H. Kang, X. Chen, J. Qian, Seismic behavior and strength capacity of steel tube-reinforced concrete composite columns, Earthquake Engineering & Structural Dynamics 43(4) (2014) 487-505.

[5] X. Ji, M. Zhang, H. Kang, J. Qian, H. Hu, Effect of cumulative seismic damage to steel tube-reinforced concrete composite columns, Earthquakes and Structures 7(2) (2014) 179-199.

[6] W.W. Qian, W. Li, L.H. Han, X.L. Zhao, Analytical behavior of concrete-encased CFST columns under cyclic lateral loading, Journal of Constructional Steel Research 120 (2016) 206-220.

[7] Simulia, ABAQUS Version 2017-1: theory manual, users' manual，verification manual and example problems manual, 2017.

[8] W. Xu, Performance of hexagonal concrete-filled steel tubular (CFST) column and the concrete-encased CFST column base, Tsinghua University, Beijing, 2016, p. 228 (in Chinese).

[9] L.H. Han, G.H. Yao, Z. Tao, Performance of concrete-filled thin-walled steel tubes under pure torsion, Thin-Walled Structures 45(1) (2007) 24-36.

[10] L.H. Han, Y.F. An, Performance of concrete-encased CFST stub columns under axial compression, Journal of Constructional Steel Research 93 (2014) 62-76.

[11] M. Attard, S. Setunge, Stress-strain relationship of confined and unconfined concrete, Materials

Journal 93(5) (1996) 432-442.

[12] L.H. Han, Tests on stub columns of concrete-filled RHS sections, Journal of Constructional Steel Research 58(3) (2002) 353-372.

[13] J.M. Shen, C.Z. Wang, J.J. Jiang, Finite element method of reinforced concrete and limited analysis of plates and shells, Tsinghua University Press, Beijing, 1993 (in Chinese).

[14] ACI, Building code requirements for structural concrete and commentary, ACI 318-14, Farmington Hills, MI, 2014.

[15] R.W. Clough, Effect of stiffness degradation on earthquake ductility requirements, Structural Engineering Laboratory, University of California1966.

[16] L.H. Han, Y.F. Yang, Cyclic performance of concrete-filled steel CHS columns under flexural loading, Journal of Constructional Steel Research 61(4) (2005) 423-452.

[17] Y. Goto, G.P. Kumar, N. Kawanishi, Nonlinear finite-element analysis for hysteretic behavior of thin-walled circular steel columns with in-filled concrete, Journal of Structural Engineering-ASCE 136(11) (2010) 1413-1422.

[18] Y.F. An, L.H. Han, Behaviour of concrete-encased CFST columns under combined compression and bending, Journal of Constructional Steel Research 101 (2014) 314-330.

[19] CECS188, Technical specification for steel tube-reinforced concrete column structure, China Planning Press, Beijing, China, 2005.

[20] M.J.N. Priestley, R. Park, Strength and ductility of concrete bridge columns under seismic loading, ACI Structural Journal 84(1) (1987).

[21] L.H. Han, Concrete-Filled Steel Tubular Structures-Theory and Practice (Third version), China Science Press, China, Beijing, 2016.

[22] J.P. Moehle, T. bavanagh, Confinement effectiveness of crossties in RC, Journal of Structural Engineering 111(10) (1985) 2105-2120.

[23] Specification of Testing Methods for Earthquake Resistant Building, China Building Industry Press, Beijing, China, 1997.

[24] CEN, Design of structures for earthquake resistance, Eurocode 8, Brussels, Belgium, 2005.

[25] W. Xu, L.H. Han, W. Li, Seismic performance of concrete-encased column base for hexagonal concrete-filled steel tube: experimental study, Journal of Constructional Steel Research 121 (2016) 352-369.

[26] L.H. Han, X.L. Zhao, Z. Tao, Tests and mechanics model for concrete-filled SHS stub columns, columns and beam-columns, Steel and Composite Structures 1(1) (2001) 51-74.

Tables

Table 1 Summary of measured and predicted results

	Specimen label	n	Δ_y(mm)		Δ_u(mm)		Measured P_{ue} (kN)	Predicted P_{uc} (kN)	P_{uc}/P_{ue}
			Measured	Predicted	Measured	Predicted			
1	CE-1	0.1	8.99	11.27	37.27	27.10	279	284	1.018
2	CE-2	0.1	9.37	11.13	36.43	32.75	285	283	0.999
3	CCS3	0.25	6.52	4.95	31.34	34.00	252	252	1.000
4	CCS4	0.25	8.38	4.62	27.73	25.98	239	242	1.012

Figures

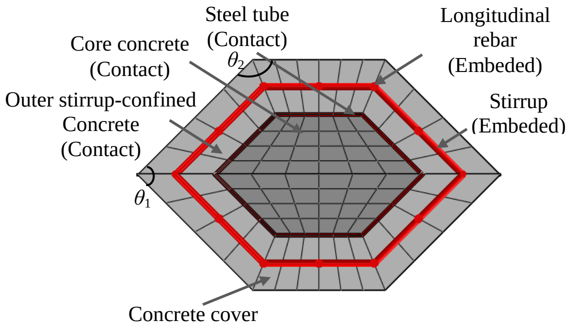

(a)FEA model-section

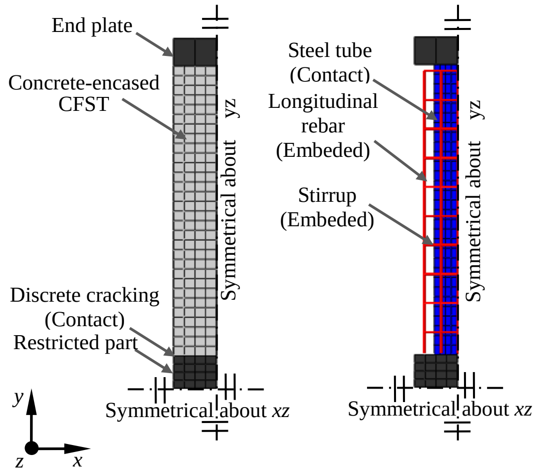

(b) FEA model-whole

Fig. 1. Schematic view of the FEA model

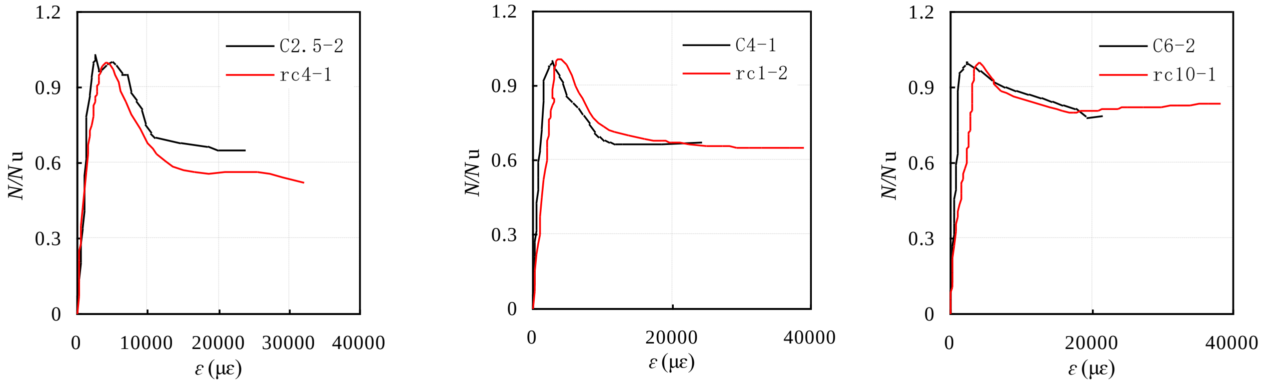

(a) =0.483 (b) =0.718 (c) =1.233

Fig. 2. Comparisons of the axial compressive behaviour of hexagonal CFST and square-section CFST

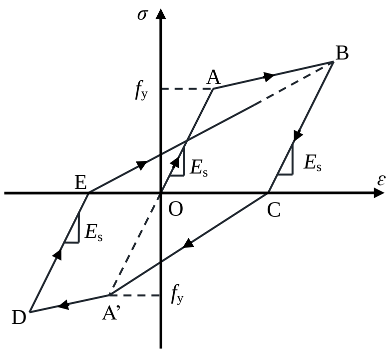

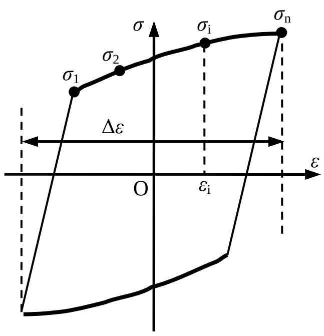

（a）Clough model （b）Combined hardening model

Fig. 3. Stress-strain relations of steel

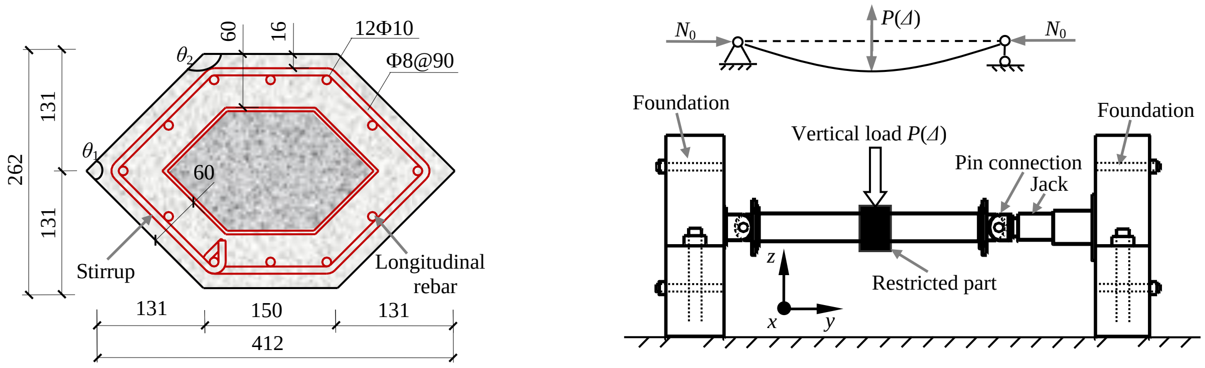

(a) Experimental section (Units:mm)　　　(b) Test setup

Fig. 4. The experimental section and test setup for Xu's test[1]

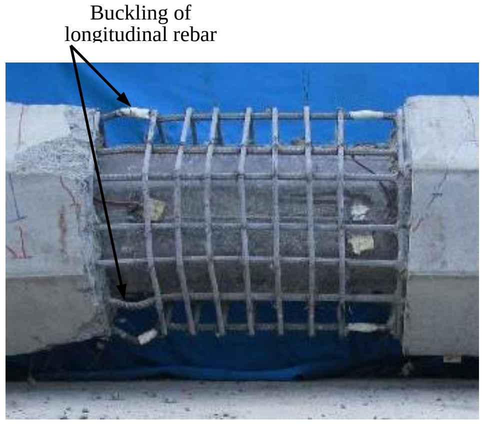

（a）CE-1 Observed

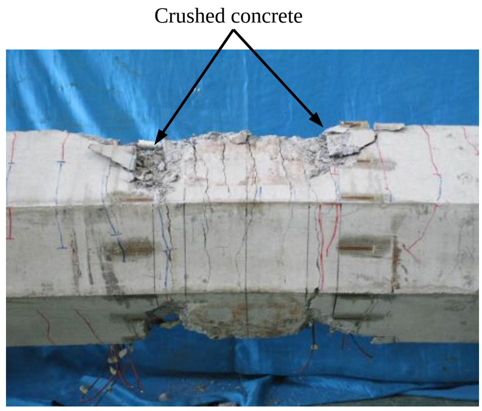

（b）CE-2 Observed

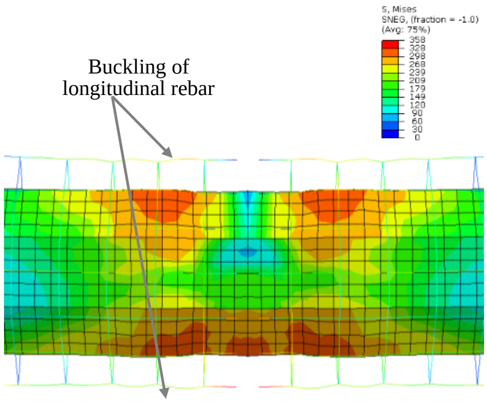

（c）CE-1 Predicted

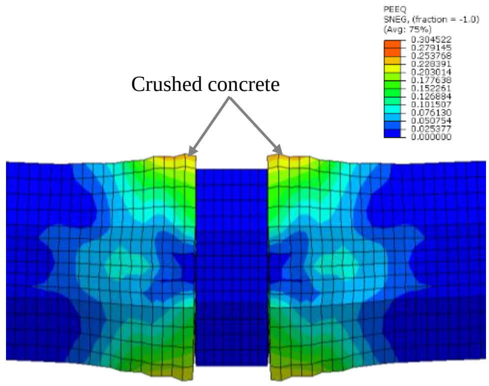

（d）CE-2 Predicted

Fig. 5. Failure mode comparisons of the experimental specimen and FEA model

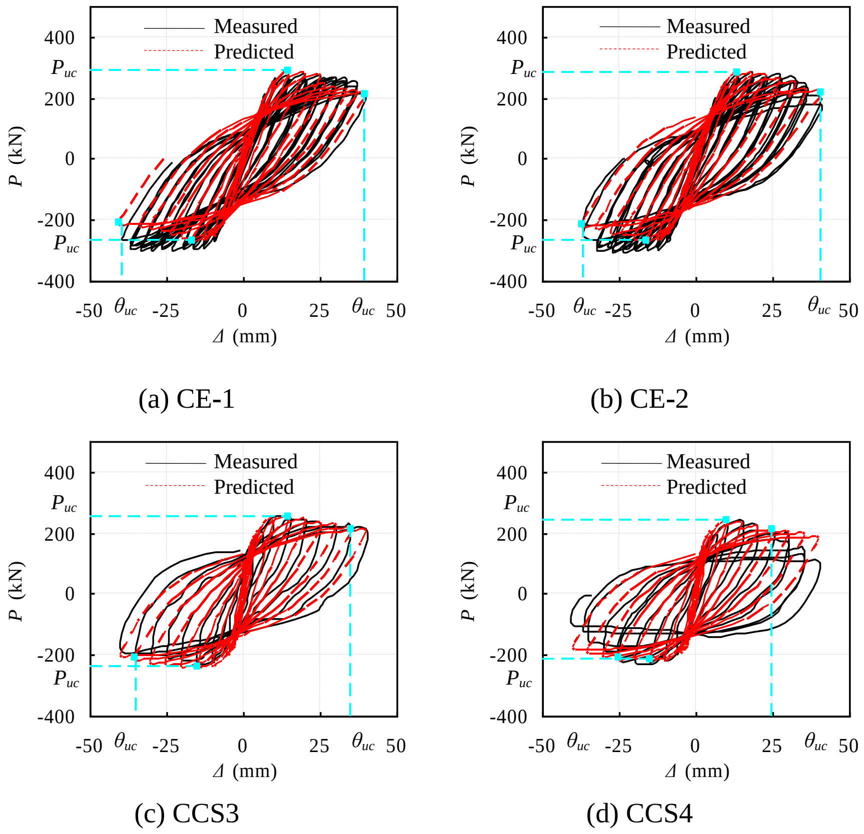

Fig. 6. Load(P) versus displacement(Δ) relations

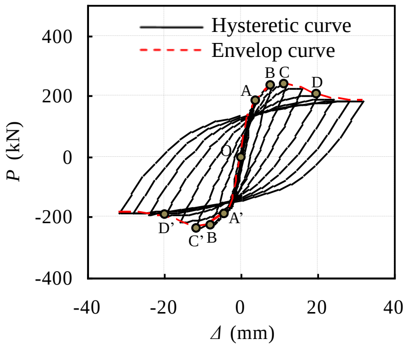

Fig. 7. Typical force-displacement relation

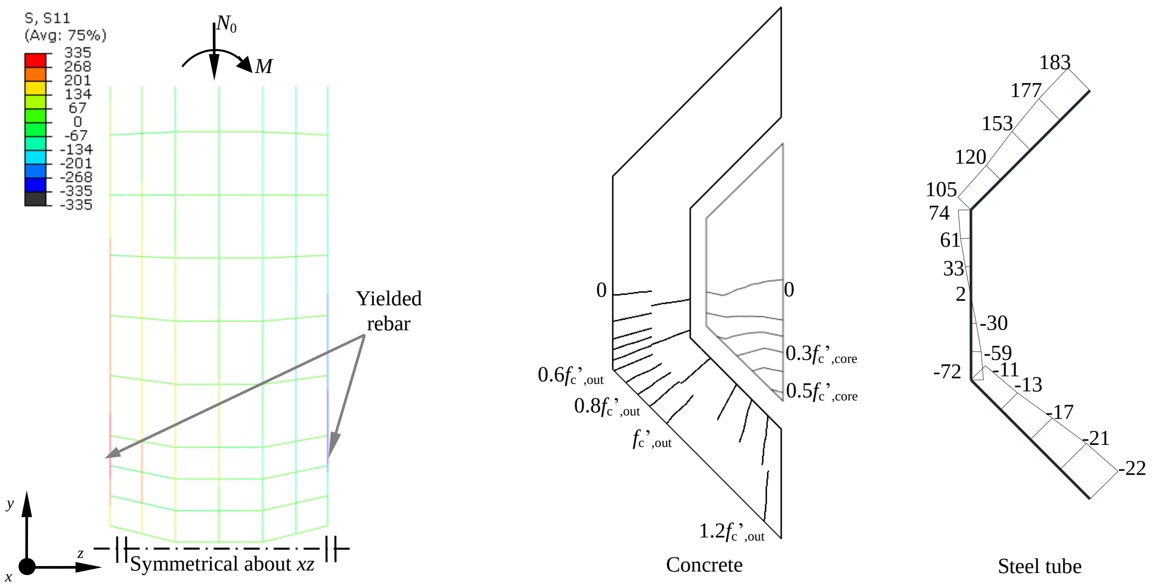

(a) Stress distribution of longitudinal reinforcements (Units: MPa)

(b) Longitudinal stress distribution of concrete and steel tube (Units: MPa)

Fig. 8. Stress of reinforcements and concrete at point A

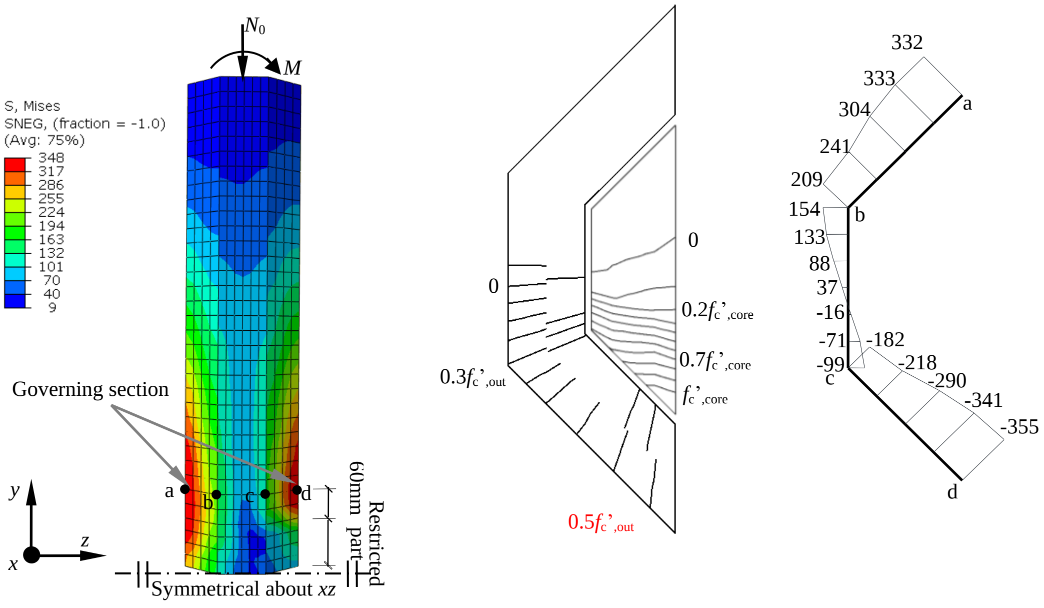

(a) von Mises stress of steel tube (Units: MPa)

(b) Longitudinal stress distribution of concrete and steel tube (Units: MPa)

Fig. 9. Stress of steel tube and concrete at point B

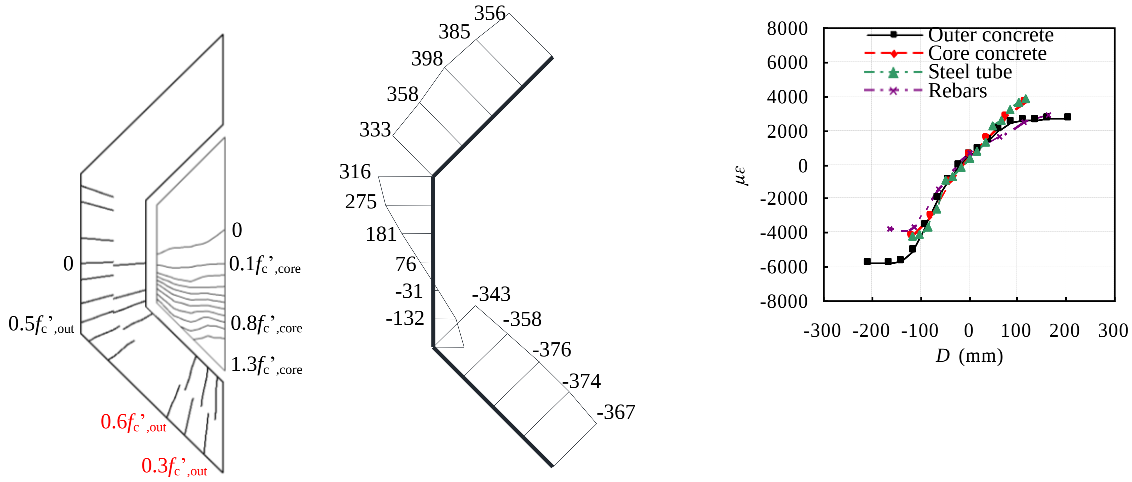

(a) Longitudinal stress distribution of steel tube and concrete (Units: MPa)

(b) Longitudinal strain distribution of all components

Fig. 10. Stress and strain distribution at point C

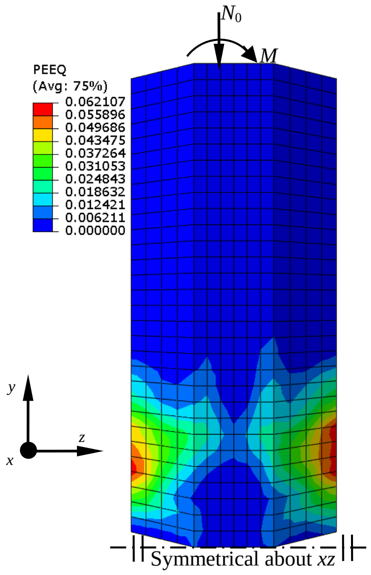

(a) Strain distribution (PEEQ) of concrete

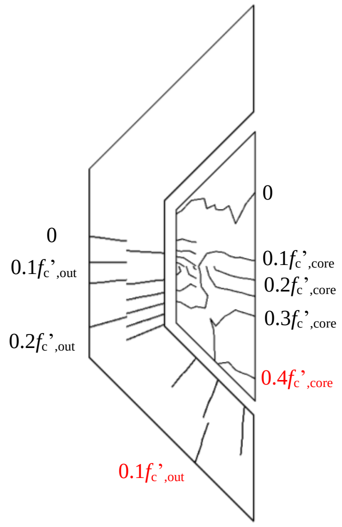

(b) Longitudinal stress distribution (S22) of concrete and (Units: MPa)

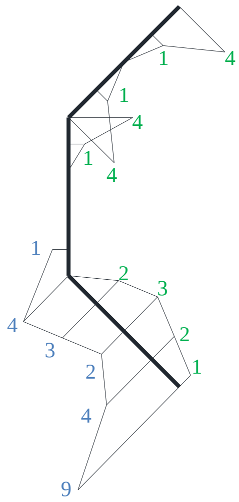

(c) Contact stress between the steel tube and concrete (Units: MPa)

Fig. 11. Stress and strain distribution at point D

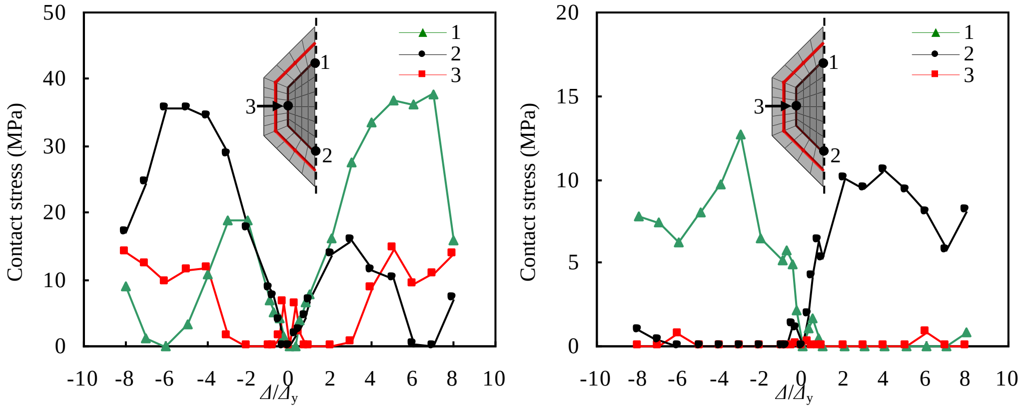

(a) Steel tube and core concrete

(b) Steel tube and outer concrete

Fig. 12. Contact stress between the steel tube and concrete in the governing section

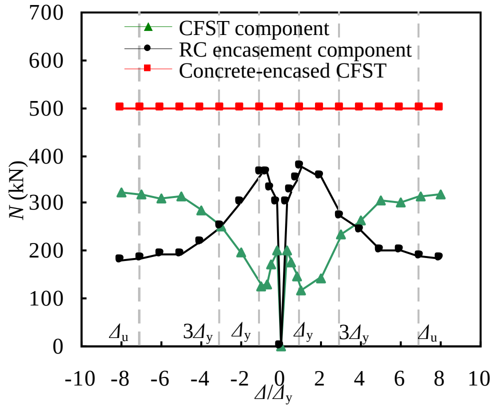

(a) Axial force

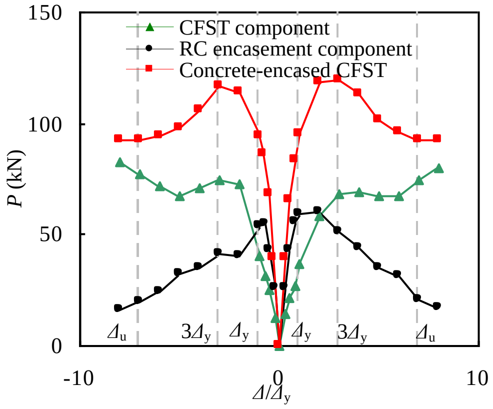

(b) Shear force

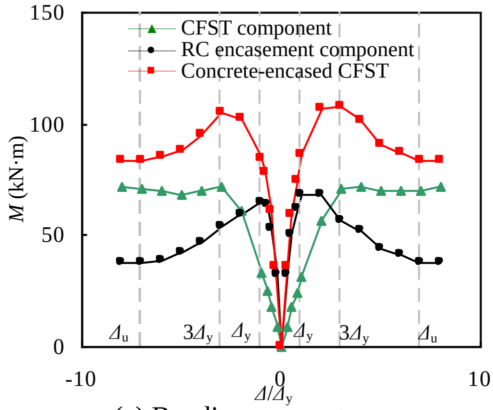

(c) Bending moment

Fig. 13. Contributions of CFST component and RC encasement component

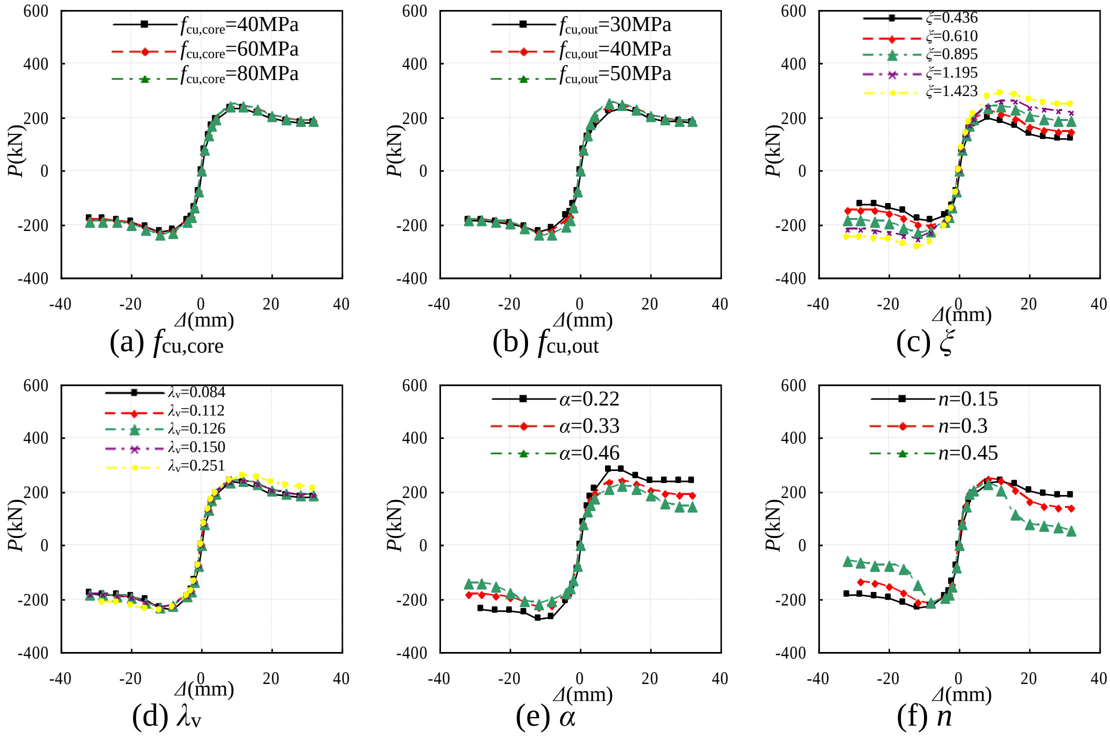

Fig. 14. Effect of different parameters on load versus displacement envelope curves

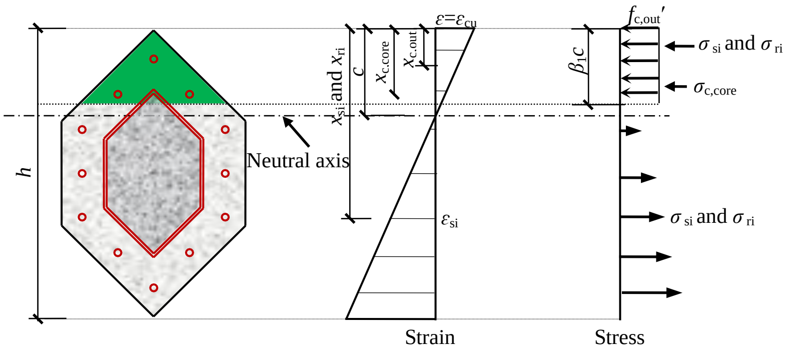

Fig. 15. Schematic view of strain and stress distributions

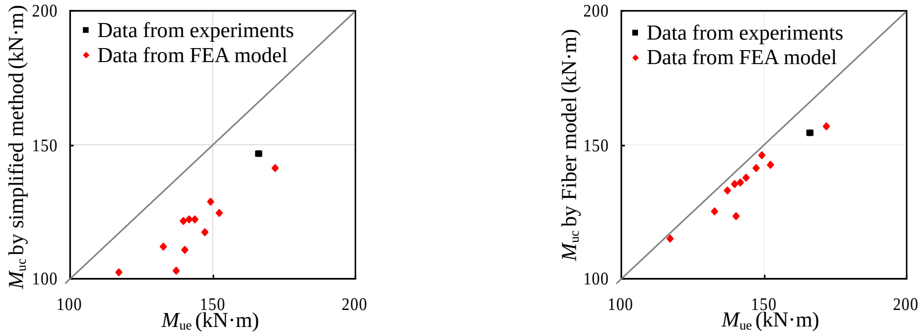

(a) Simplified method (b) Fiber model

Fig. 16. Comparisons between measured and predicted flexural strength